High-Sensitivity Organic Upconversion Photodetectors for Near-Infrared Photoplethysmography

Peixian Lei[1], Zeyu He[1, 2], Xiaoyang Du[1], Silu Tao[1, *]

[1]School of Optoelectronic Science and Engineering, University of Electronic Science and Technology of China, Chengdu 611731, China

[2]Shimmer Center, Tianfu Jiangxi Laboratory, Chengdu 641419, China

[*] Corresponding author: Silu Tao _ silutao@uestc.edu.cn

Abstract

Near-infrared photoplethysmography (PPG) plays a critical role in noninvasive monitoring of arterial pulse and cardiovascular function. However, conventional organic near-infrared photodetectors are intrinsically limited by insufficient photodetection capability and noise suppression capability, making it highly challenging to simultaneously achieve high sensitivity, low noise, and high signal readability under low-light conditions. Here, we propose and demonstrate an organic electrically driven upconversion (UPC) strategy, in which weak near-infrared optical signals are upconverted into visible light and subsequently reabsorbed within the device, enabling signal amplification and high-fidelity readout at the device level. Under an applied bias of 10 V, the UPC device exhibits an external quantum efficiency of 134% at 835 nm, a responsivity of 0.90 A/W at 840 nm, and a specific detectivity of 3.7 × 10^{12} Jones. Benefiting from these outstanding optoelectronic properties, the PPG system based on this UPC device can clearly resolve arterial pulse waveforms, including systolic peaks, diastolic valleys, and distinct dicrotic notches. These results demonstrate the device's high sensitivity to biological pulse signals and provide a new physical pathway and engineering paradigm for the design of high-performance organic photodetectors in biomedical monitoring applications.

Keywords

Near-infrared, photodetector, arterial monitoring, photoplethysmography, biomedical monitoring.

1. Introduction

Photoplethysmography (PPG) is a widely adopted noninvasive optical technique for real-time monitoring of cardiovascular parameters such as heart rate, blood flow dynamics, and vascular elasticity[1]. In particular, near-infrared (NIR) illumination is highly desirable for PPG measurements due to its deeper tissue penetration and reduced scattering compared with visible light[2]. In recent years, organic NIR photodetectors have attracted increasing attention in wearable bioelectronics owing to their advantages of lightweight construction, mechanical flexibility, large-area fabrication, and spectral tunability[3].

Despite these advantages, organic photodetectors still face fundamental limitations in practical NIR-PPG applications. The relatively weak NIR absorption of organic semiconductors and limited charge separation efficiency often result in low output signal amplitudes[4]. Meanwhile, attempts to enhance responsivity by increasing operating bias or device thickness typically lead to elevated dark current and noise levels, which severely degrade the signal-to-noise (SNR) ratio and obscure fine pulse waveform features[5]. Although external electronic amplification circuits can be employed to boost signal amplitude, they inevitably introduce additional noise,

increase power consumption, and complicate system integration. Therefore, achieving effective amplification and high-fidelity readout of weak NIR physiological signals directly at the device level remains a critical and unresolved scientific challenge in organic photodetection[6].

Electrically driven upconversion (UPC) devices offer an alternative signal-processing paradigm beyond conventional photodetectors[7]. By electrically coupling a NIR photodetection unit with a visible-light emission unit, weak NIR signals can be upconverted into visible photons[8]. Importantly, the emitted visible light can be reabsorbed by the photodetection layer, generating additional charge carriers and thereby enabling intrinsic signal amplification and optical readout within a single device architecture. This strategy has the potential to overcome the SNR limitations of standalone photodetectors while enabling integrated optical signal transduction.

In this work, we construct an organic electrically driven UPC device by integrating a PM6:Y6-based NIR photodetection unit with a red-emitting $Ir(MDQ)_2(acac)$-based electroluminescent unit. The optoelectronic properties of the device are systematically investigated. The device achieves an EQE exceeding 90% over a broad spectral range from 400 to 900 nm, together with a responsivity of 0.90 A/W at 840 nm and a detectivity of 3.7×10^{12} Jones, demonstrating pronounced electrical gain and effective noise suppression. Furthermore, when applied to PPG signal acquisition, the device enables clear resolution of pulse waveform features including systolic and diastolic components, confirming its high sensitivity to weak hemodynamic signals.

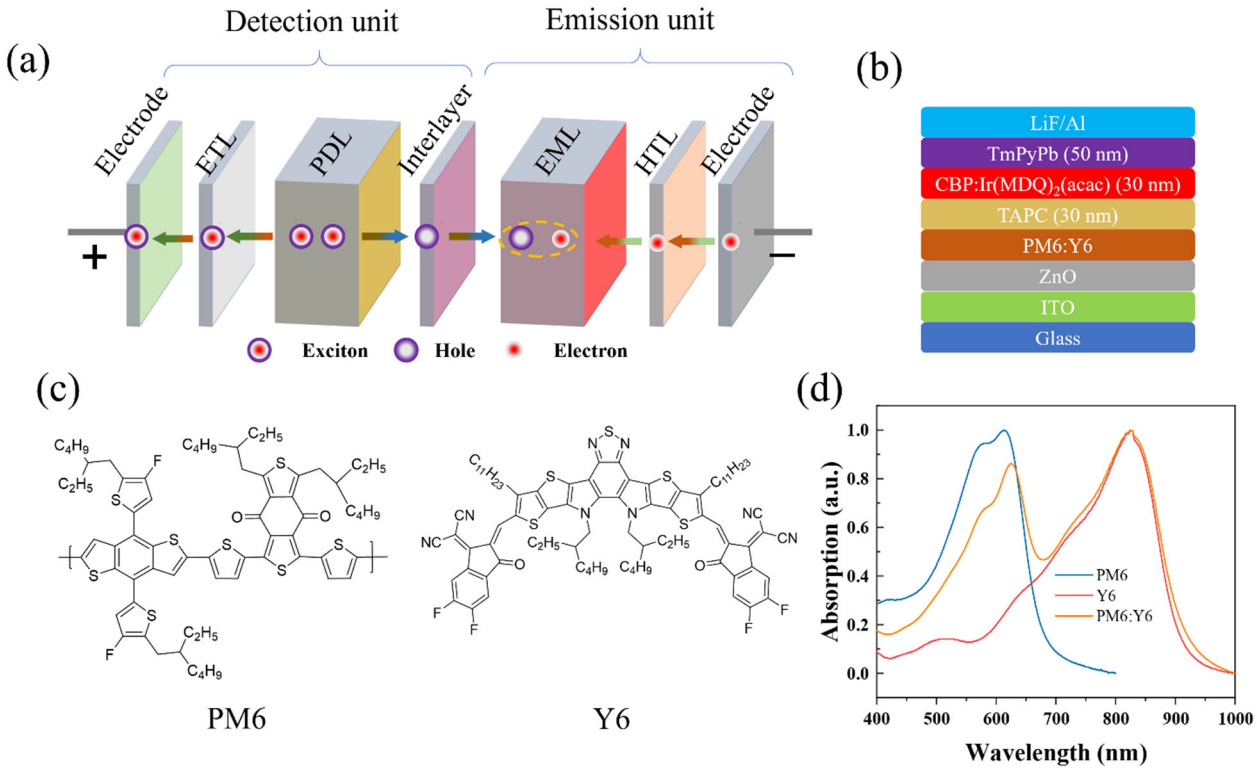

Figure 1. (a) The operating principle and carrier transport pathways of the UPC. (b) The architecture of the UPC. (c) The molecular structures of PM6 and Y6. (d) The absorbtion spectrm of PM6, Y6 and PM6:Y6 blend film.

2. Results

A. Device Structure and Working Principle

Fig. 1a illustrates the operating principle and carrier transport pathways of the UPC. Upon NIR illumination, photons are absorbed by the photodetection layer (PDL), where excitons are generated and subsequently dissociated into free charge carriers at the donor–acceptor

interface between PM6 and Y6. Under an applied bias, photogenerated holes are driven through the interlayer toward the emission layer (EML), where they recombine radiatively with injected electrons to produce visible red emission. Notably, the emitted visible photons can be reabsorbed by the PDL, generating additional charge carriers and thereby contributing to internal signal amplification.

The architecture of the UPC is shown in Figure 1b and consists of glass/ITO/ZnO/PM6:Y6/TAPC (30 nm)/CBP:Ir(MDQ)$_2$(acac) (30 nm)/TmPyPb (50 nm)/LiF (0.8 nm)/Al (120 nm). The ZnO serves as the electron transport layer and hole-blocking layer due to its deep valence band, effectively suppressing hole leakage and reducing dark current. The PDL is prepared using a solution method, with PM6 and Y6 (Fig. 1c) mixed in a 1:1.2 mass ratio to form a high-efficiency bulk heterojunction, ensuring reliable near-infrared detection. As shown in Fig. 1d, the absorption spectra of the acceptor materials, Y6 exhibit strong NIR absorption extending from 600 to 900 nm, with distinct peaks centered at 813 nm. The donor polymer PM6 exhibits absorption from 400 to 700 nm with pronounced peaks located at 575 and 612 nm. the PM6:Y6 blend exhibits strong absorption from 300 to 900 nm, enabling broadband NIR detection[9]. TAPC functions as an interlayer with well-matched energy levels, facilitating efficient hole transport from the PDL to the EML. The emission layer consists of a commercial host material doped with the red phosphorescent emitter Ir(MDQ)$_2$(acac), while TmPyPb ensures efficient electron injection from the cathode.

B. Performance of the Photodetection Unit

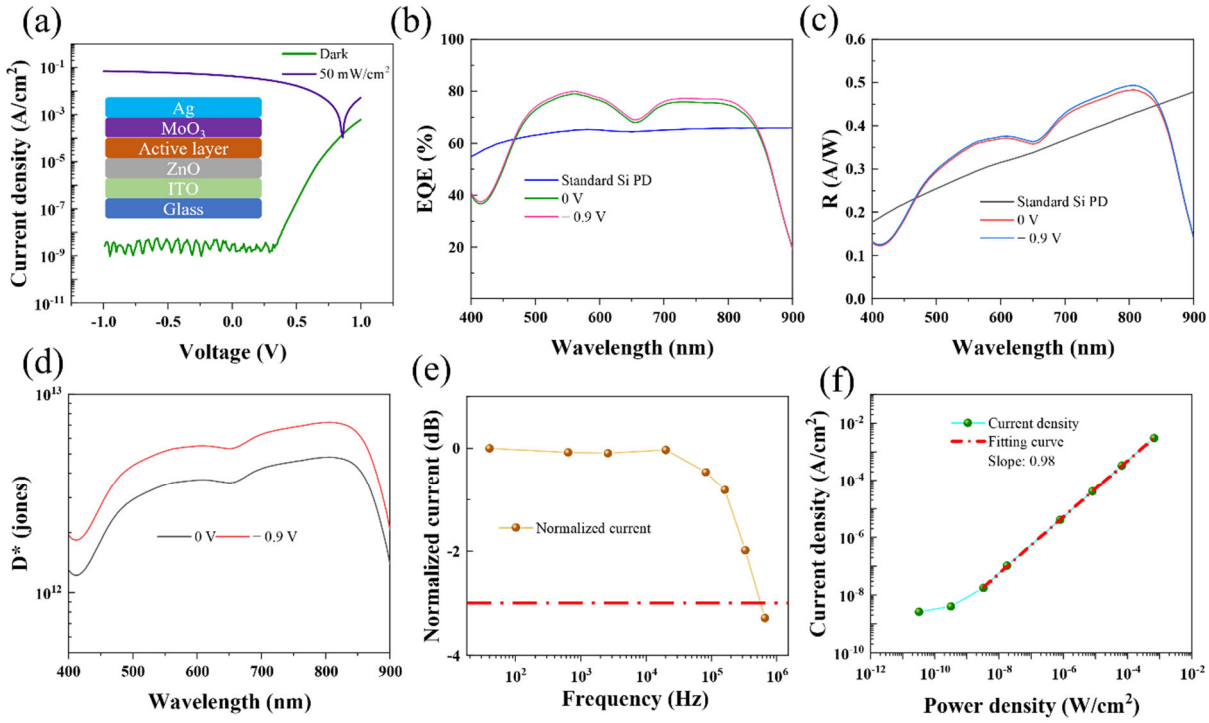

Figure 2. (a) The typical dark and illuminated I–V characteristics of the photodetection unit, inset shows structure of photodetection unit. (b) The EQE spectum of the photodetection unit. (c) The R of the photodetection unit. (d) The D* of the photodetection unit. (e) Normalized photocurrents as function of modulating frequency of the photodetection unit. (f) LDR of the photodetection unit under illumination of 520 nm light.

To systematically evaluate the photodetection performance, standalone photodetector devices were fabricated and characterized. Fig. 2a presents the typical dark and illuminated current–voltage (I–V) characteristics. The photodetection unit were fabricated with a structure of ITO/ZnO/PM6:Y6/MoO_3/Ag, as shown in inset of Fig. 2a. Under 808 nm illumination with a

power density of 50 mW/ cm^2, the device achieves an on/off current ratio of up to 5 × 10^6, indicating excellent photosensitivity and a wide dynamic response range.

Fig. 2b shows the EQE spectra measured under zero bias and reverse bias conditions. The EQE exceeds 60% across the wavelength range from 460 to 840 nm, outperforming standard photodetectors and confirming efficient photoresponse. Based on the EQE, the responsivity (R) is calculated, as shown in Fig. 2c. At 810 nm, the responsivity reaches 0.48 A/W at 0 V and increases slightly to 0.49 A/W at −0.9 V. The specific detectivity (D*) is also derived from the EQE and dark current characteristics (Fig. 2d), yielding values of 4.8 × 10^{12} Jones at 815 nm and 0 V, and 7.2 × 10^{12} Jones at −0.9 V.

In addition to static performance metrics, the temporal response of the photodetector was evaluated. As shown in Fig. 2e, a −3 dB cutoff frequency of 6 × 10^5 Hz is achieved at 520 nm under zero bias, indicating fast response suitable for dynamic sensing. Furthermore, the linear dynamic range (LDR), a critical parameter for imaging and sensing applications, reaches an impressive 104 dB with a fitted linear slope of 0.98, demonstrating excellent linearity over a wide range of incident light intensities.

C. Performance of the Emission Unit

To evaluate the electroluminescent performance of the red emission unit, standalone OLED devices were fabricated with a structure of ITO/TAPC (30 nm)/CBP:Ir(MDQ)$_2$(acac) (30 nm)/TmPyPb (50 nm)/LiF/Al, as shown in Fig. 3a. The device exhibits a low turn-on voltage of approximately 3.2 V. As the driving voltage increases from 3 to 10 V, both current density and luminance increase monotonically, reaching a maximum luminance of approximately 1.6 × 10^4 cd/m^2 at 10 V (Fig. 3b), indicating efficient carrier injection and radiative recombination.

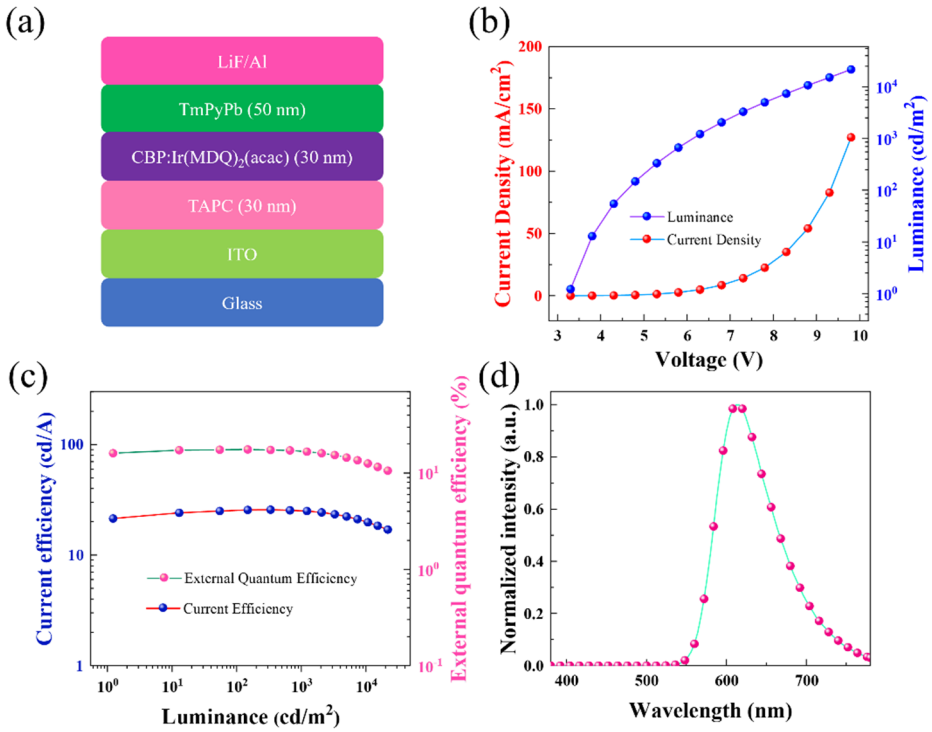

Figure 3. (a) The architecture of the emission unit. (b) J–V–L curves, (c) CE–L–EQE curves, (d) electroluminescence spectra of the emission unit.

As shown in Fig 3c, the current efficiency reaches a peak value of approximately 25 cd/A, corresponding to an EQE of about 20%, and remains relatively stable over a luminance range of 1–3000 cd/m^2. At higher luminance levels, efficiency roll-off is observed, which can be

attributed to exciton–exciton annihilation and enhanced nonradiative recombination under high carrier density. As shown in Fig. 3d, the electroluminescence spectrum exhibits a stable emission peak centered at approximately 612 nm with a narrow full width at half maximum, confirming that the emission originates from the characteristic phosphorescence of $Ir(MDQ)_2(acac)$. These results demonstrate that the red OLED provides high brightness, high efficiency, and spectral stability, making it a reliable visible-light output unit for the UPC device.

D. Performance of the Upconversion Device and PPG Demonstration

The electrical characteristics of the UPC device were further investigated. As shown in Fig. 4a, dark current and photocurrent measurements were performed under dark conditions and 808 nm illumination. The device exhibits a stable and low dark current density; as the bias voltage increases from 0 to 10 V, the dark current density remains below 1.0×10^{-7} A/cm^2, owing to the low dark current of the photodetection subunit and the effective energy barriers provided by ZnO and the emission subunit. Under 808 nm illumination, an on/off ratio of 1.0×10^5 is achieved.

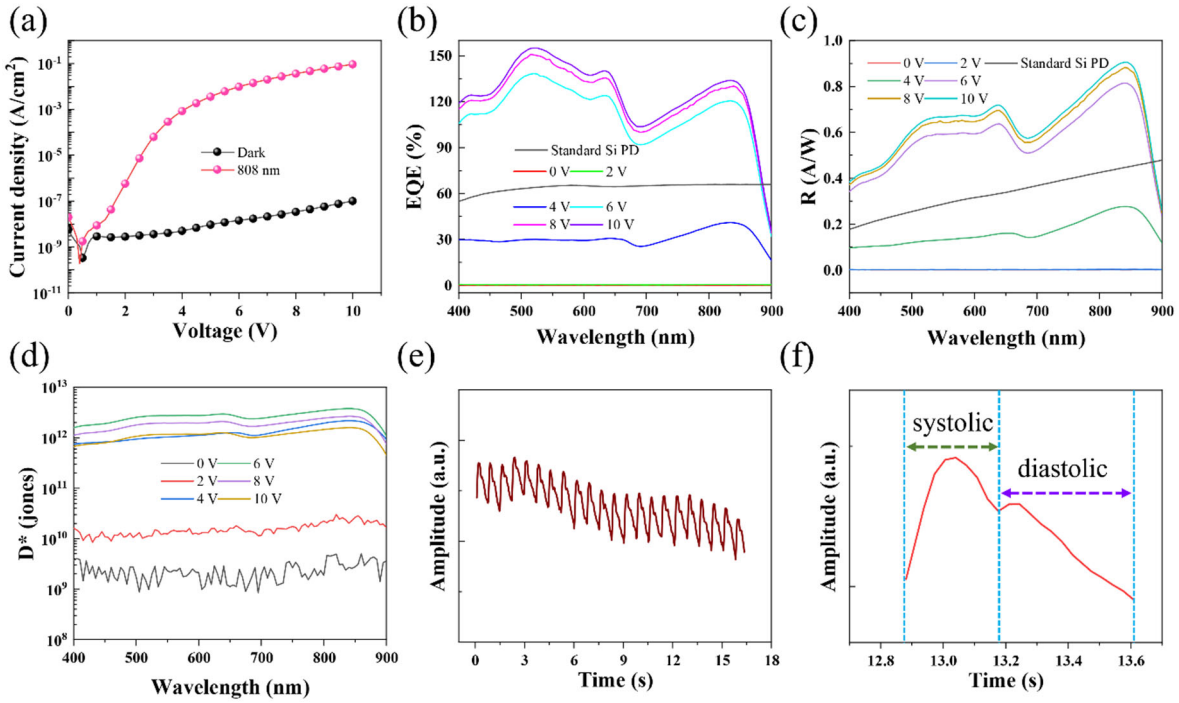

Figure 4. (a) The typical dark and illuminated I–V characteristics of the UPC. (b) The EQE spectum of the UPC at different reverse bias . (c) The R of the UPC at different reverse bias. (d) The D* of the UPC at different reverse bias. (e) Time-domain PPG signals recorded by UPC under 1064 nm illumination. (f) LDR of the photodetection unit under illumination of 808 nm light. (f) The single PPG signal.

Fig. 4b shows the bias-dependent EQE spectra, which increase with applied voltage. At biases above 6 V, the EQE exceeds 90% across the wavelength range from 400 to 850 nm. Notably, an exceptionally high EQE of 134% is obtained at 835 nm under a bias of 10 V. The corresponding responsivity and detectivity are shown in Fig. 4c and 4d, respectively. At 10 V, the device achieves a responsivity of 0.90 A/W and a detectivity of 3.7 × 10^{1}2 Jones at 840 nm. These outstanding values are attributed to bias-assisted carrier transport and the internal optical–electrical gain enabled by the upconversion architecture.

Given the excellent performance of the UPC, human pulse measurements were conducted to demonstrate its practical applicability. As shown in Fig. 4e, under 808 nm illumination with a

power density of 5 mW/cm^2, the device continuously records human pulse signals with a signal amplitude of approximately 4.6 μA. The pulse waveform is clearly resolved, yielding a pulse period of approximately 0.75 s and a heart rate of about 80 beats per minute. A magnified view of a single pulse cycle (Fig. 4f) reveals rich waveform details, allowing clear distinction between systolic and diastolic periods of approximately 0.3 s and 0.5 s, respectively. These results demonstrate that the UPC enables high-fidelity pulse monitoring comparable to clinically invasive arterial measurements.

3. Conclusion

In conclusion, we demonstrate an organic electrically driven upconversion device in which photogenerated holes are transported through an interlayer to the emission layer, where they recombine with injected electrons to produce red emission. The emitted red photons can be reabsorbed by the photodetection layer, generating additional charge carriers and thereby enhancing the overall detection performance. Under a bias of 10 V, the device achieves an EQE of 134% at 835 nm, a responsivity of 0.90 A/W at 840 nm, and a detectivity of 3.7×10^{12} Jones. The PPG system based on this device can clearly resolve arterial pulse waveforms, including systolic peaks, diastolic valleys, and dicrotic notches. These results not only demonstrate a novel design strategy for organic upconversion devices but also validate their high sensitivity for biological pulse monitoring, offering a new physical pathway and engineering paradigm for high-performance organic photodetectors in wearable biomedical applications.

4. Materials Information and Device Fabrication

Materials: The PM6 and Y6 were purchased from Solarmer Materials Inc. (Beijing). TAPC, CBP, Ir(MDQ)$_2$(acac), PmPyPB and LiF were purchased from Luminescence Technology Corp. MoO_3 were purchased from Sigma-Aldrich Inc. All reagents and solvents were used directly as received.

Device Fabrication: The ZnO was spin-coated on the cleaned ITO substrates by using sol-gel strategy with speed of 5000 rpm and then were transferred to a hot plate immediately for thermal annealing (200 °C, 1h). The PM6:Y6 film prepared on ZnO in the glove box with a speed of 3000 rpm by utilizing solution process (PM6:Y6 were dissolved in CF, w:w = 1:1.2) with concentration of 15 mg/ml,. They were transferred to a vacuum evaporation chamber (10^{-5} Pa) and TAPC, CBP: Ir(MDQ)$_2$(acac), PmPyPB, LiF/Au were sequentially deposited on the PM6:Y6 film. All electrical characteristics data recorded using a Keithley 2400 source meter. EQE spectrums were obtained by using a QEX10 System. All optical characteristics data were recorded by a Spectrascan PR655 photometer. All tests were conducted in an atmospheric environment.

Acknowledgment

The work was supported by the National Natural Science Foundation of China (NSFC grant no. 62474028, 52130304 62222503 and 62505040), the Natural Science Foundation of Sichuan Province (2025ZNSFSC0037, 2026NSFSC1445 and 2025ZNSFSC1460). National Key R and D Program of China (2023YFB2604101). This work was also sponsored by the Sichuan Province Key Laboratory of Display Science and Technology.

References

[1] Lou, Z., Tao, J., Wei, B., Jiang, X., Cheng, S., Wang, Z., Qin, C., Liang, R., Guo, H., Zhu, L., Müller-Buschbaum, P., Cheng, H., & Xu, X. (2023). Near-infrared organic photodetectors toward skin-

integrated photoplethysmography-electrocardiography multimodal sensing system. Advanced Science, 10(36), 2304174. https://doi.org/10.1002/advs.202304174.

[2] Yang, Y., Chen, Y., Pei, P., Fan, Y., Wang, S., Zhang, H., Zhao, D., Qian, B.-Z., & Zhang, F. (2023). Fluorescence-amplified nanocrystals in the second near-infrared window for in vivo real-time dynamic multiplexed imaging. Nature Nanotechnology, 18(10), 1195–1204. https://doi.org/10.1038/s41565-023-01432-8

[3] Chandran, H. T., Huang, J., Xia, H., Nair, R. R., Xing, S., Li, G., Leo, K., & Benduhn, J. (2025). Beyond silicon: Toward sustainable, NIR-II, and conformable organic photodiodes. Advanced Energy Materials, e04357. https://doi.org/10.1002/aenm.202504357

[4] Ren, H., Chen, J., Li, Y., & Tang, J. (2021). Recent progress in organic photodetectors and their applications. Advanced Science, 8(1), 2002418. https://doi.org/10.1002/advs.202002418

[5] Chow, P. C. Y., & Someya, T. (2020). Organic photodetectors for next-generation wearable electronics. Advanced Materials, 32(15), 1902045. https://doi.org/10.1002/adma.201902045

[6] Che, Z.-L., Yan, C.-C., Wang, X.-D., & Liao, L.-S. (2024). Organic near-infrared optoelectronic materials and devices: An overview. Advanced Photonics, 6(01). https://doi.org/10.1117/1.AP.6.1.011301

[7] He, Z., Du, X., Zheng, C., Yu, X., Lin, H., & Tao, S. (2023). High-quality artery monitoring and pathology imaging achieved by high-performance synchronous electrical and optical output of near-infrared organic photodetector. Advanced Science, 10(2), 2203870. https://doi.org/10.1002/advs.202203870

[8] Zhang, Y., He, Z., Du, X., Han, J., Lin, H., Zheng, C., Wang, J., Yang, G., & Tao, S. (2022). High-performance organic upconversion device with 12% photon to photon conversion efficiency at 980 nm and bio-imaging application in near-infrared region. Optics Express, 30(10), 16644. https://doi.org/10.1364/OE.457911

[9] Zhu, H., Jia, Z., Liu, T., Xiong, Q., Lai, Y., & Yang, Y. M. (2025). Simultaneous enhancement of narrowband detection and suppression of dark current in organic near-infrared photodetectors via second-order resonant microcavity. Laser & Photonics Reviews, e01187. https://doi.org/10.1002/lpor.202501187